Journal of Applied Fluid Mechanics, Vol. 16, No. 6, pp. 1232-1242, 2023.
Available online at www.jafmonline.net, ISSN 1735-3572, EISSN 1735-3645.
https://doi.org/10.47176/jafm.16.06.1683

Numerical Study of the Effect of a Power-law Fluid Flow Structures on Levels of Mixing in a Taylor Couette Configuration

S. Khali† and R. Nebbali

USTHB – Faculty of Mechanical and Process Engineering (FGMGP), Laboratory of Multiphase Transport and Porous Media (LTPMP), B.P.32, El Alia Bab Ezzouar 16111, Algiers, Algeria

†*Corresponding Author Email: samir.khali@usthb.edu.dz*

(Received November 27, 2022; accepted February 1, 2023)

ABSTRACT

This work is a numerical study on the effects of the flow structures of the power-law fluid between two concentric cylinders with an upward laminar axial flow on levels of mixing and mean residence time through the Taylor Couette system. The cylindrical annular duct presents a radius ratio of 0.5 and an aspect ratio of 8. The inner cylinder is rotating while the outer one is kept at rest. The residence time distributions (R.T.D.) method and the mean residence time (Tm) are used to determine the number of tanks in series and the dispersion coefficient to evaluate levels of mixing. To this end, a pulsed input injection of a tracer is computing at the outlet of the annulus. As a main objective of this study, is to analyze the effect of the flow structure of a power-law fluid between two concentric cylinders on the mixing level and mean residence time in a Taylor Couette system. The novelty of our work is the use of power-law fluids as particles-carrying fluids. Several parameters, such as the axial Reynolds number (Re), the Taylor number (Ta), and the power-law index behavior (n), are used to show their impact on levels of mixing. It is shown that when n increases, the number of stirred tanks in series N increases for pseudoplastic fluids (n<1), indicating low levels of mixing while the parameter (N) decreases for dilatants fluids (n>1), revealing high levels of mixing. The increase of the power-law index in the range of 0.6<n<1 decreases the dispersion coefficient, indicating the non-ideal mixing in the duct. In addition, for further increase of the power-law index in the range of n>1 increases the dispersion coefficient points to the well-mixing.

Keywords: Poiseuille-Taylor-Couette flow; Residence time distribution; Meantime; Lattice Boltzmann Method; Non-Newtonians fluids.

NOMENCLATURE

c	lattice Velocity	Δt	time step set to unity
C	dimensionless concentration	Δz	lattice space size set to unity
C_α	particle distribution function for the concentration	δ_{ij}	Kronecker function
		ν	fluid kinetic viscosity
C^{eq}	equilibrium distribution Function for the concentration	ε	error
		ω_α	Weight coefficients for the equilibrium distribution function
C_s	sound speed		
d	gap of the annular duct	ρ	fluid density
D	coefficient of the mass diffusion	τ_α	relaxation time of the D2Q9 lattice Boltzmann equation along direction α
e_α	Particle velocity vector along direction α		
$E(t)$	residence time distribution	τ	relaxation time of the D2Q9 lattice Boltzmann equation
F_α	particle distribution function		
F^{eq}	equilibrium distribution Function	$\overline{\tau}$	relaxation time of the D2Q4 lattice Boltzmann equation for azimuthal velocity
G_α	particle distribution function for the azimuthal velocity		
G^{eq}	equilibrium distribution Function for the azimuthal velocity	τ_c	relaxation time of the D2Q4 lattice Boltzmann equation for the concentration
Gr	Grashof number		
I_α	source term added into lattice Boltzmann	Γ	Aspect ratio $\Gamma = L/(R_2 - R_1)$

	equation
K_α	source term added to the azimuthal velocity equation
k	consistence of the non-Newtonian fluid
lu	lattice spacing (spatial lattice unit)
lt	lattice time step (temporal lattice unit)
L	height of the annulus
M	Mach number
N	number of tanks agitated in series
n	power-law index behavior
p	pressure
R_1	radius of the inner cylinder
R_2	radius of the outer cylinder
Re	Reynolds number
S_α	source term added into lattice Boltzmann equation
Sc	Schmidt number
t	time
Ta	Taylor number
T_m	meantime
v_r	Radial velocity
v_θ	azimuthal velocity
v_z	axial velocity
w(z)	laminar axial velocity

Greek Symbol

α	thermal diffusion coefficient
η	radius ratio
μ_a	apparent viscosity for non-Newtonians fluids
$\partial\alpha$	partial space derivative, α can represent z or r
Φ	source term added into lattice Boltzmann equation
γ	source term added into lattice Boltzmann equation
$\dot{\gamma}$	shear rate
Ω	angular speed of the inner cylinder
σ	first moment of the distribution function
σ^2	second moment of the distribution function
δ_x	lattice spacing lu (m) set to unity
δ_t	lattice time step lt (s) set to unity
Δt	time step lu, (s) set to unity

Subscripts

α	component in direction e_α
α, β	axial coordinate z or radial coordinate r
z ,r	axial and radial coordinates respectively
w	wall
α_{op}	opposite direction of α.

1. INTRODUCTION

Levels of mixing and mean residence time of non-Newtonians fluids through the different apparatus is an important key parameter for the design and the efficiency of various reactors in industrial apparatuses involved in mechanical engineering, chemical engineering and oil drilling. The residence time distribution (R.T.D.) is a model used to characterize levels of mixing, and defined as the time each particle of a tracer remained in the channel. Results in distributions of the tracer injection at the output are used to get fluid levels of mixing. For a Dirac-Delta function of the R.T.D, the tracer enters and leaves simultaneously the channel, signifying a plug flow. On the other hand, when the R.T.D., exhibits an exponential decay function, the flow describes a good mixing. Danckwerts (1958) was first to use the R.T.D method as a new technique to quantify the levels of mixing by injecting a tracer in the Taylor-Couette configuration. Kataoka *et al.* (1975) uses the residence time distribution to study the fluid flow structures for the Taylor Vortex Flow regime (T.V.F.) between two concentric cylinders. They ended that each vortex behaves as a perfectly agitated reactor and does not interact with the adjacent vertices. This work is considered as a reference study for the subsequent studies such as Legrand *et al.* (1983), Legrand and Coeuret (1986) and Guihard *et al.* (1989). Kataoka and Takigawa (1981) proposed a new model to quantify leveling of mixing as the number of tanks in series N. They described each reactor by a number N of perfectly mixed tanks in series. When the number of tanks in series is equal to one, the flow is perfectly mixed and when N tends to infinity, the flow is a plug flow.

For the Taylor-Couette system, the dispersion coefficient model is often used to show how the fluid is mixed. The tracer drifts along the radial direction due to the centrifugal forces and the R.T.D widens, and the flow describes a plug flow. A high dispersion coefficient reveals the decrease of radial concentration gradients along the radial direction, and flow is well mixed. Kataoka *et al.* (1977) showed that the dispersion coefficient through the Taylor Couette configuration becomes independent of the molecular diffusion coefficient and increases with the imposed axial flow. Their results were confirmed later by Enkoida *et al.* (1989) and Moore and Cooney (1995). Pudjioni and Tavar (1993) predicted experimentally the dispersion coefficient through Couette flow device. For a given flow rate, the authors determine a critical Taylor number as a function of the dispersion coefficient. Tam and Swinney (1987) and Ohmura *et al.* (1997) carried out an experimental study based on the piston reactor model to determine the axial dispersion coefficient for several flow regimes in Taylor Couette configuration. Legentilhomme *et al.* (1997) analyzed the impact of the addition of a phase dispersion of microcapsules on the residence time distribution of a liquid phase through an annular channel. Desmet *et al.* (1996) showed by the R.T.D that the convection dominates in the zone close to the separation region between the vortices, while the diffusion dominates in the center of the vortices. One year later, Campero and Vigil (1997) used a similar approach that led to a three parameters model to study the non-ideal mixing in the central zone of the vortices, as suggested by Desmet *et al.* (1996). Zhu *et al.* (2000) identify the limits of the classical model of non-perfectly stirred reactor.

Nemri *et al.* (2016) carried out a numerical and experimental study of the mixing properties of several Taylor-Couette flow regimes by using the axial dispersion coefficient model and R.T.D measurements. They confirmed the significant effect of the flow structure on the axial dispersion and mixing properties. Among studies using the R.T.D for different geometries, we quote Zhang *et al.* (1990), Madeira *et al.* (2006), Haicheng *et al.* (2022), Gyürkes *et al.* (2022) and Wang *et al.* (2022). Guo *et al.* (2018) conducted experimental and theoretical study to show the effectiveness of the R.T.D for multichannel apparatus. Their results show that the R.T.D model is a useful technique for the diagnosis of flow distribution non-uniformity through multichannel devices. Aparicio-Mauricioa *et al.* (2020) showed that the combination of experimental R.T.D with C.F.D modeling is an effective approach to understand and visualize the hydrodynamic behavior and mass transport.

The mean age theory is another method, which provides the distribution of the average time of all particles crossing a given position and estimates levels of mixing in different tanks. It received a particular interest in the literature, we cite Baleo and Cloirec (2000), Bartak *et al.* (2002), Chanteloup and Mirade (2009), Liu and Tilton (2010) and Russ and Berson (2016). They used a derivative of the mean age theory to characterize the flow of oil, water, and air through pipelines to characterize the age profiles for each phase. Their works showed that the average age could be applied to the individual phases. Theaker (2017) compares residence time distributions with mean age theory in systems by varying the number of stirred tanks in series model. Liu (2011) developed a map of the spatial mean age distributions as a function of the tank diameter, with the objective to identify critical parameters influencing the mean age. Among studies concerning non-Newtonian fluids, one can cite Kaur and Gupta (2022); Kaur *et al.* (2022); Devi and Gupta (2022); Devi et al. (2022) and Shukla and Gupta (2022).

As conclusion, it appears numerical studies carried out the residence time distribution in the Taylor – Couette system involving Power-law non-Newtonians fluids with the presence of an axial laminar flow are rare. In our work, a pulse injection of a tracer is computed numerically at the outlet of the Taylor Couette configuration with a radius ratio of 0.5 and an aspect ratio of 8 as it is shown in the Fig. 1. The inner cylinder is rotating while the outer cylinder is maintained at rest. Different influencing parameters, such as the Taylor number, the axial Reynolds number and the power-law index behavior can be reflected by R.T.D response curve. The dispersion coefficient and the number of stirred tanks to give valuable information such as the power law fluid flow structure and mixing levels.

2. GOVERNING EQUATIONS

The lattice Boltzmann equation for the axial and the radial velocity component in the D2Q9 model for axisymmetric, laminar and incompressible flow is: Zhou (2011).

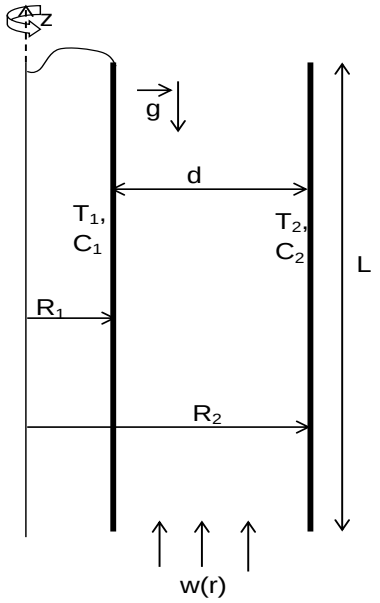

Fig. 1. Physical domain.

$$F_\alpha(z+c_{\alpha z}\delta_t, r+c_{\alpha r}\delta_t, t+\delta_t) = F_\alpha(z,r,t) + \tau_\alpha\left[F_\alpha^{eq}(z,r,t) - F_\alpha(z,r,t)\right] + \gamma\Delta t + \phi_\alpha(z,r,t) \quad (1)$$

The lattice Boltzmann equation for the azimuthal velocity in the (D2Q4) model is: Zhou (2011)

$$G_\alpha(z+\bar{c}_{\alpha z}\delta_t, r+\bar{c}_{\alpha r}\delta_t, t+\delta_t) - G_\alpha(z,r,t) = \frac{1}{\bar{\tau}}\cdot\left[1+\frac{(2\bar{\tau}-1)\bar{c}_{\alpha r}\Delta t}{2r}\right]\left[G_\alpha^{eq}(z,r,t) - G_\alpha(z,r,t)\right] + I_\alpha(z,r,t) \quad (2)$$

The lattice Boltzmann equation for the concentration field in the D2Q4 model is:

$$C_\alpha(z+\bar{c}_{\alpha z}\delta_t, r+\bar{c}_{\alpha r}\delta_t, t+\delta_t) - C_\alpha(z,r,t) = \frac{1}{\tau_C}\cdot\left[1+\frac{(2\tau_C-1)\bar{c}_{\alpha r}\Delta t}{2r}\right]\left[C_\alpha^{eq}(z,r,t) - C_\alpha(z,r,t)\right] \quad (3)$$

F_α, G_α and C_α are respectively the density, the azimuthal velocity and the concentration distribution functions. F_α^{eq}, G_α^{eq} and C_α^{eq} are the equilibrium distribution functions along α directions for respectively the axial and the radial velocities, the azimuthal velocity and the concentration field. τ_α, $\bar{\tau}$ and τ_C are respectively the relaxation times in the α direction for the flow fields, the azimuthal velocity and the concentration. γ, ϕ_α, I_α are source terms.

For D2Q9 LBGK model components of the discrete velocity vector are given as follows: Zhou (2011)

$$c_\alpha = \begin{cases} (0,0) & \alpha = 0 \\ \left(\cos\left[\frac{(\alpha-1)\pi}{2}\right], \sin\left[\frac{(\alpha-1)\pi}{2}\right]\right)c & \alpha = 1,2,3,4 \\ \sqrt{2}\left(\cos\left[\frac{(\alpha-5)\pi}{2}+\frac{\pi}{4}\right], \sin\left[\frac{(\alpha-5)\pi}{2}+\frac{\pi}{4}\right]\right)c & \alpha = 5,6,7,8 \end{cases} \quad (4)$$

The expression of the relaxation time τ_α and the equilibrium distribution function F_α^{eq} are defined as Zhou (2011):

$$\tau_\alpha = \frac{1}{\tau} + \frac{(2\tau-1)c_{\alpha r}\Delta t}{2\tau r} \quad (5)$$

$$F_\alpha^{eq}(z,r,t) = \omega_\alpha \frac{p}{c_s^2} + \omega_\alpha \rho \left[\frac{c_\alpha v}{c_s^2} + \frac{(c_\alpha v)^2}{2c_s^4} - \frac{v^2}{2c_s^2}\right] \quad \alpha = 0,1,2,...,8, \quad (6)$$

$c_s = c/\sqrt{3}$ is the sound velocity and ω_i are weight coefficients given as ω_α =4/9, ω_α=1/9 for α=1, 2, 3, 4 and ω_α=1/36 for α=5, 6, 7, 8.

For D2Q4 LBGK model the weight coefficients $\omega\alpha$ are equal to 1/4, and the discrete velocity vector of a particle is given by

$$\bar{c}_\alpha = c\left[\cos\frac{(\alpha-1)\pi}{2}, \sin\frac{(\alpha-1)\pi}{2}\right], \alpha = 1,2,3,4 \quad (7)$$

The expression of the equilibrium distribution functions for the azimuthal velocity in the equation (2) and for the concentration in the equation (3) is defined as: Zhou (2011)

$$G_\alpha^{eq}(z,r,t) = \left[1 + \frac{2\bar{c}_\alpha v_j}{\bar{c}_s^2}\right]\frac{\rho v_\theta}{4} \quad (8)$$

$$C_\alpha^{eq}(x,t) = R\omega_\alpha . C\left[1 + \frac{\bar{c}_\alpha . v}{c_{sr}^2}\right] \quad (9)$$

$c = \delta_x/\delta_t$ is the sound speed set to the unity, δ_x and δ_t are respectively the lattice spacing and time step and set to unity.

The relationship between the relaxation time and the fluid viscosity ν in the D2Q9 model is: $\nu = (2\tau-1)\delta_x/6$ and for the D2Q4 model is: $\nu = 0.5\left(\bar{\tau} - 0.25\right)$.

The apparent viscosity of the power-law fluids is:

$$\mu_a = k\left|\dot{\gamma}\right|^{(n-1)} \quad (10)$$

$\dot{\gamma}$ is the local shear rate, n is the power-law fluid index and k is the fluid consistency.

The corresponding dimensionless of the density, velocities, and the concentration are obtained as follows:

$$\rho(z,t) = \sum_\alpha F_\alpha(z,t), \; v_\theta = \frac{1}{\rho}\sum_\alpha G_\alpha,$$
$$\rho v(z,t) = \sum_\alpha c_\alpha F_\alpha(z,t), \quad (11)$$
$$C = \sum_\alpha C_\alpha(z,t)$$

The residence time distribution function noted E(t) is calculated at the outlet of the annulus and is given as: Wang *et al.* (2022)

$$E(t) = \frac{c(t)}{\int_0^\infty c(t)dt} \quad (12)$$

The mean residence time t_m is considered as the first moment of the distribution function and has the following expression: Wang *et al.* (2022)

$$t_m = \int_0^\infty tE(t)dt \quad (13)$$

The variance of the distribution (σ^2) corresponds to the second moment of the distribution function and is given as: Wang *et al.* (2022)

$$\sigma^2 = \int_0^\infty (t-t_m)^2 E(t)dt \quad (14)$$

The number (N) of tanks agitated in series is determined by the following relation: Zhang *et al.* (1990)

$$N = \frac{t_m^2}{\sigma^2} \quad (15)$$

The dispersion coefficient is linked to the Peclet number by the following expression: Theaker (2017)

$$D = \frac{UL}{Pe} \quad (16)$$

The Peclet number (Pe) is obtained by the following expression: Theaker (2017)

$$\frac{\sigma^2}{t_m^2} = \frac{2}{Pe} - \frac{2}{Pe^2}\left(1 - e^{-Pe}\right) \quad (17)$$

2.1 Boundary Conditions

At the entrance of the annulus, the boundary conditions for the axial laminar flow are:

$$\rho = (F_0 + F_1 + F_3 + 2(F_4 + F_7 + F_8)) / (1 - w(r))$$
$$F_2 = F_4 + (2/3)\rho w(r)$$
$$F_5 = F_7 + (1/6)\rho w(r) - (1/2)(F_1 - F_3) \quad (18)$$
$$F_6 = F_8 + (1/6)\rho w(r) - (1/2)(F_3 - F_1)$$

Where the velocity profile equation of w(r) is:

$$w(r) = \left(\frac{1}{4\mu}\right)\left(-\frac{dp}{dz}\right)\left[\frac{\left(R_2^2 - R_1^2\right)}{\ln(\eta)}\ln\left(\frac{R_2}{R}\right) - \left(R^2 - R_2^2\right)\right] \quad (19)$$

On the outer cylinder, we used the bounce-back rule of the non-equilibrium distribution:

$$F_1 = F_3 + (F_1^{eq} - F_3^{eq})$$
$$F_5 = F_7 + (F_5^{eq} - F_7^{eq}) \quad (20)$$
$$F_8 = F_6 + (F_8^{eq} - F_6^{eq})$$

On the inner cylinder, all the distribution functions were taken equal to their corresponding equilibrium distribution functions to prevent slipping condition: Zhou (2011)

$$F_\alpha = F_\alpha^{eq} \quad , \quad G_\alpha = G_\alpha^{eq} \quad (21)$$

No mass flux exchanges condition is used for the concentration fields on the top, the inner and the outer boundaries: Zhou (2011)

$$C_\alpha = C_{\alpha_{w-1}} \quad (22)$$

Where, α_{w-1} is the nearest mesh layer of the wall.

At the bottom of the duct, the boundary condition for the concentration field is: Khali *et al.* (2017)

$$C_\alpha = C_w\left(\omega_i + \omega_{i_{op}}\right) - C_{\alpha_{op}} \quad (23)$$

3. NUMERICAL RESULTS

Due to the complexity of the physical phenomena involved in our study, all the calculations were carried out by setting the aspect ratio to 8 and the radius ratios to 0.5. The axial Reynolds number is taken equal to 3 and 6. The Taylor number based on the rotating inner cylinder is taken equal to 30, 80 and 100, which correspond, respectively, to the laminar stable regime (C.F.), onset of Taylor cells and the laminar instable regime (T.V.F.). The power-law index behavior (n) is varied in the range 0.6 and 1.4. Pseudo-plastics fluids correspond to n<1, dilatants fluids correspond to n>1 and n=1 stands for the Newtonian fluid. 20 lattice nodes in the radial direction and 160 nodes in the axial direction mesh of the physical domain of the Fig.1. In addition, the lattice size is set to 1, and the time step is equal to unity.

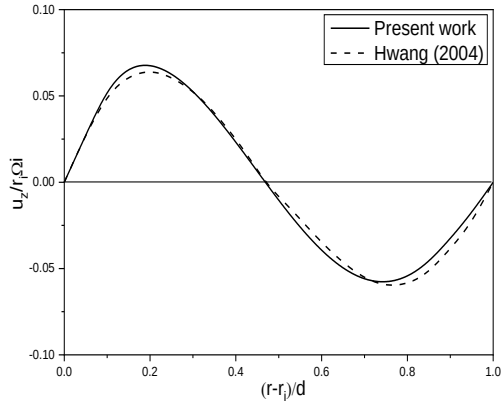

(a)

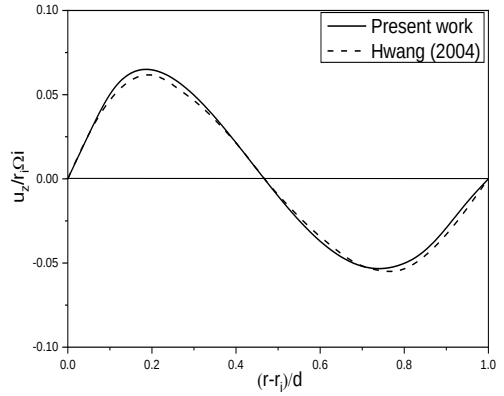

(b)

Fig. 2. Velocity axial component along the radial direction for Ta=120, η=0.8, Γ=14.3, Re=0 and 4.9. (a): Ta=123 and Re=0, (b): Ta=123 and Re=4.3.

As any numerical simulation, a convergence criterion of our L.B.M. code is adopted to stop the computational process when the following convergence criterion is satisfied as reported in Khali *et al.* (2017):

$$\sum_{i,j} \frac{\left\| v(x_{i,j} + c_\alpha \delta_t, t + \delta_t) - v(x_{i,j}, t) \right\|}{\left\| v(x_{i,j} + c_\alpha \delta_t, t + \delta_t) \right\|} < 10^{-6} \quad (24)$$

Where i, j are the lattice nodes indices.

Before any use of the present code, a process of verification and validation has been conducted. First, Fig. 2 shows a confrontation between the evolution of the axial velocity along the radial direction for Ta= 123 with, and without an imposed axial laminar of our present work and the velocity profile of Hwang and Yang (2004). It emerges a good concordance between our results and those of Hwang and Yang (2004) where the mean absolute error does not exceed 9.84% for the Fig. 2(a), and 7.5% for the Fig. 2(b). Second, Fig. 3 presents the comparison of the Sherwood number along the parameter $(z / D_h \, Re \, Sc)$ with that obtained with the correlation reported in Molki *et al.* (1990) for Ta=0, Re=120, η=0.5 and n=1. The result reveals a good agreement. Finally, Fig. 4 shows the result of a

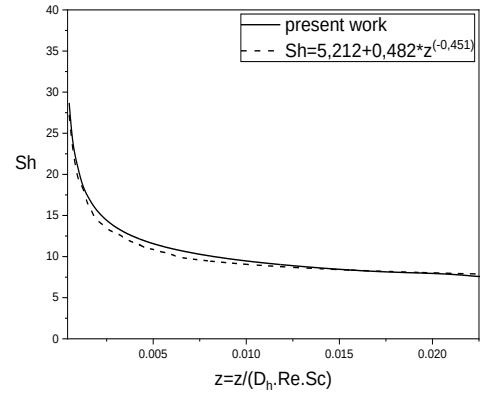

Fig. 3. Distribution of the Sherwood number for Ta = 0, Re= 120, η=0.5 and n=1.

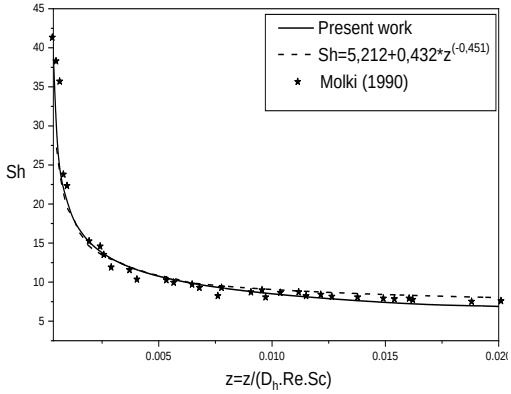

Fig. 4. Distribution of Sherwood number of Newtonian fluid (n=1) for Ta = 100, Re= 120, η=0.5.

confrontation of the Sherwood number distribution along the parameter $(z / D_h \, Re \, Sc)$ with that of the correlation of $Sh = 5.212 + 0.432\, z^{(-0.451)}$.

Figure 5 illustrates the distribution of the Sherwood number for a Newtonian fluid of n=1 along the axial direction without an axial flow (Re=0) and for Ta=80 and 100. The Sherwood number exhibits high values at the entrance of the annulus because of the high gradients of concentration. Then, the Sherwood number decreases along the length of the duct as the boundary layer grow, reducing, therefore, the mass transfer intensity. Figure 5 shows also the effect of the inner cylinder rotation on the mass transfer rate. In fact, increasing the rotation of the inner cylinder of Ta=100 produces the increase of the mass transfer rate. This increase occurs due to the presence of Taylor cells in the duct. The value of the Taylor number of Ta=100 reveals a quite different trend. In fact, the Sherwood number exhibits a sinusoidal shape. For Ta=80, the Sherwood number remains almost constant, denoting the dominance of the axial viscous forces, due to the axial flow, on the centrifugal forces, due to the rotation of the inner cylinder.

The impact of the fluid rheological behavior on the mass transfer rate is illustrated in Fig. 6 for Re=3 and Ta=100. We note that the rate of mass transfer

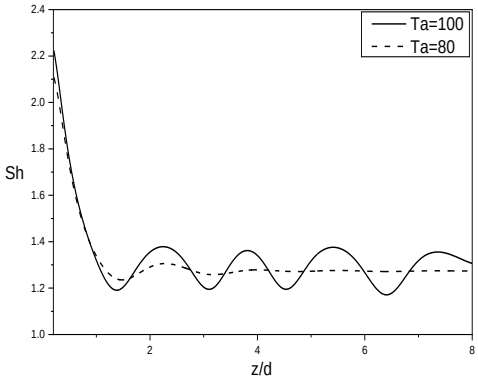

Fig. 5. Distribution of the Sherwood number for the Newtonian fluid (n=1) along the axial direction without axial flow (Re=0) and for Ta=80 and 100.

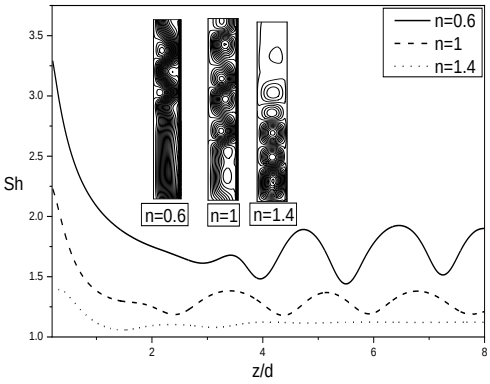

Fig. 6. Evolution of the Sherwood number for n=0.6, n=1, and n=1.4 along the axial direction for Re=3 and Ta= 100.

decreases when the power-law index (n) increases, attributed to the fluid apparent viscosity increase. The Sherwood number shows oscillating shape in the axial direction for the pseudo-plastic fluid (n=0.6) and the Newtonian fluid (n=1). For dilatant fluids (n=1.4) we note that the Sherwood number is lower in the annulus due to the dominance of the centrifugal forces on the axial viscous forces.

Figure 7 shows the Sherwood number evolution for a Newtonian fluid (n=1) for different values of the axial Reynolds number and a Ta= 80. We note Taylor cells disappear in the annulus when the axial Reynolds number increases. Without an axial flow (Re=0), Taylor cells are present in the annulus and the Sherwood number exhibits a sinusoidal form in the area where these vortices extend. The increase in the Reynolds number has damping effects on the Taylor vortices growth and, therefore, it reduces the mass transfer rate in the channel.

The evolution of the residence time distribution for a dilatant fluid of n=1.2 for Ta=30 and for Re=3 and 6 is shown in Fig. 8. We note that the curve's peak of the residence time distribution is higher when the axial Reynolds number is equal to 6. The peak residence time increases when the axial viscous forces increase and prevails on the

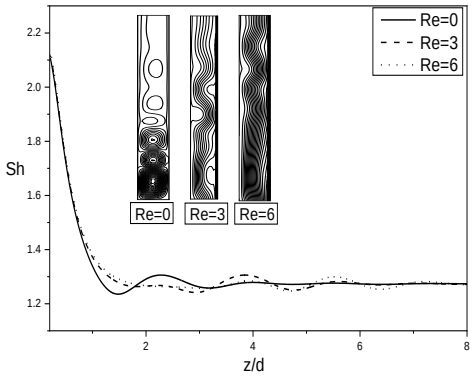

Fig. 7. Evolution of the Sherwood number for Newtonian fluid (n=1) for different values of the Reynolds number along the axial direction for Ta= 80.

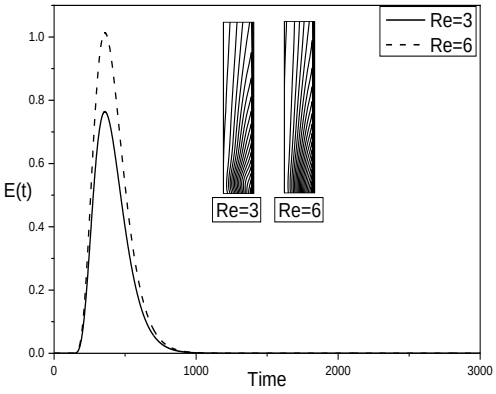

Fig. 8. Evolution of the residence time distribution for two values of Reynolds number (Re=3 and 6) for Ta=30 and n=1.2.

centrifugal forces in the annulus, leading to a low level of mixing in the duct.

The Fig. 9 illustrates the resident time distribution for a dilatant fluid of n=1.2 for two values of the Taylor number (80 and 100) and Re=3. We note that the peak of the R.T.D curves decreases with the increase of the Taylor number due to the presence of Taylor cells in the annulus. In addition, for Ta=80 we observe the dominance of the axial pressure gradient on the centrifugal forces and as a result, the tracer enters and leaves more rapidly than for Ta=100 where the flow exhibits a T.V.F. regime. As a result, the flow is well mixing for Ta=100 than Ta=80.

Figure 10 shows the combined effect of the Taylor and axial Reynolds numbers on the mean residence time as a function of the power-law index fluid behavior (n). The variation of the mean residence time shows an increase with the power-law index (n) before experiencing a decrease after reaching a maximum value for pseudoplastic fluids ($0.8 < n < 0.9$). For Re=3 in Fig. (10a), we note that the mean residence time is slightly higher for a lower Taylor number for fluids belonging to the pseudoplastic family because; the axial flow dominates the secondary flow generated by the inner cylinder

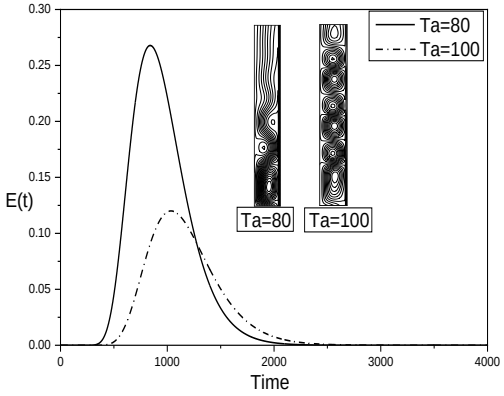

Fig. 9. Evolution of the residence time distribution of a dilatant fluid (n=1.2) for Ta=80, Ta=100 and Re=3.

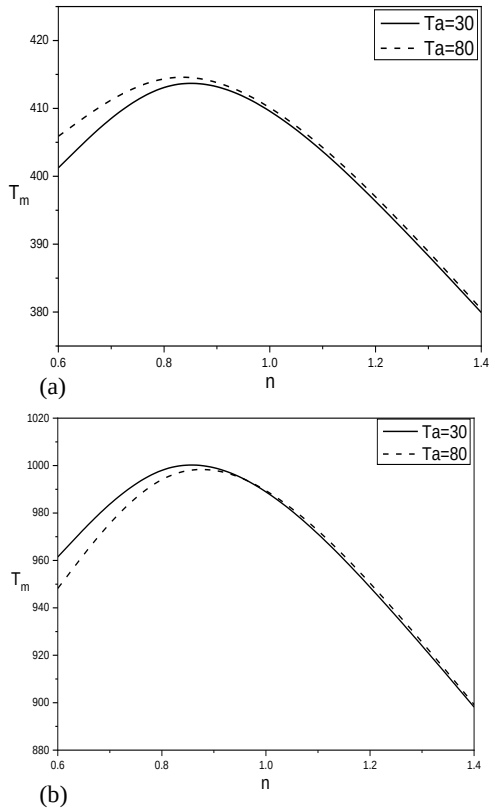

Fig. 10. Evolution of the mean residence time for different values of n for Ta=30 and 80. (a): Re=3, (b) : Re=6 .

rotation. For Re=6 (Fig. 10b) the opposite trend is observed for pseudo-plastics fluids for Ta= 30 and Ta=80 while for dilatants and Newtonian fluids the mean residence time is almost the same.

Figure 11 shows the evolution of mean residence time as a function of the power-law index (n) for Ta= 80. We notice that T_m is 2.5 times higher for Re=3 than for Re=6. When Re=3, the flow structure is characterized by the presence of Taylor cells surrounded by an axial lines flow, which increases the residence time of the tracer crossing the duct. Unlike for Re=6, the cells disappear, which shortens the path experienced by the tracer

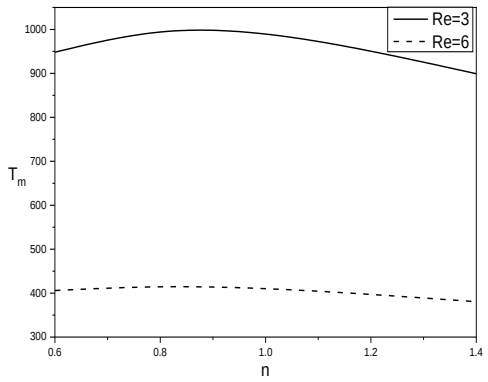

Fig. 11. Evolution of the mean residence time as a function of the power-law index (n) for Re=3 and 6 and Ta= 80.

reducing, therefore, the mean residence time too. In addition, for constant values of the Taylor number, both of the axial Reynolds number values and the mean residence time is less sensitive to the power law index (n).

Figure 12 illustrates the distribution of the residence time distribution of different rheological power-law fluids for Ta=80 and Re=3. We notice that the area under the curves of the residence time distribution increases when the power-law index (n) increases. In fact, increasing n leads to the higher apparent viscosity of the fluid, thereby reducing the axial viscous forces, which allows the Taylor cells to grow in size and gain in intensity. Thus, when n increases, gradients of the concentration increase along the radial direction and leading to higher levels of mixing.

Figure 13 shows residence time distributions for different radius ratios for Ta=100, n=1.2, and Re=3. We note that when the radius ratio increases, the peak value of the R.T.D curves increase in the annulus. In fact, the increase of the radius ratio reduces the annular gap, lowering thus the centrifugal force intensity, and as a result, the Taylor cells vanished in the duct for the higher value of the radius ratio and the flow tends to non-mixing.

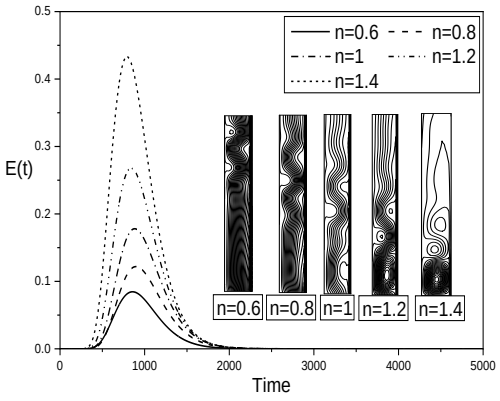

Fig. 12. Evolution of the residence time distribution of different rheological fluids for Ta=80 and Re=3.

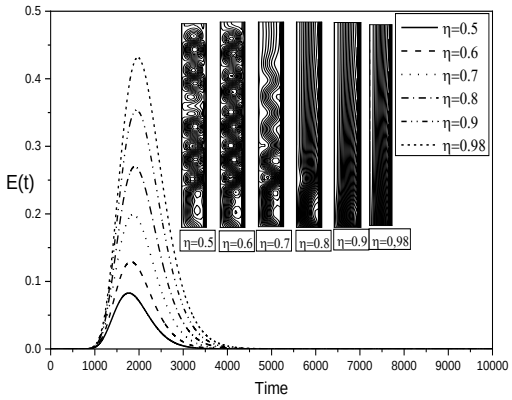

Fig. 13. Evolution of the residence time distribution for different radius ratios for different aspect ratio for Ta=100, n=1.2 and Re=3.

The Fig. 14 shows the variation of the number of tanks in series (N) versus the rheological power-law index (n) for Ta=100 and for both values of the axial Reynolds number, Re=3 and 6. The number (N) of tanks-in-series is a model that is used to quantify levels of mixing. From the Fig. 14, we note that N increases and exhibits a similar trend that observed for T_m in the Fig. 10. In addition, when the power-law index increases, pseudoplastic fluids (n<1) require higher N indicates a lower level of mixing while dilatant fluids (n>1) need a less number of N which indicates a higher level of mixing.

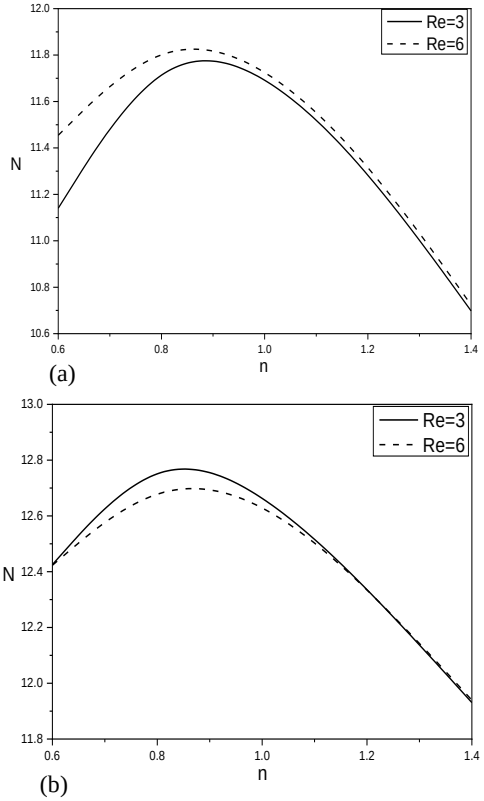

Fig. 14. Evolution of the equivalent number of stirred tanks in series for a dilatant fluid (n=1.2) for Re=3 and 6. (a): Ta=30 and (b): Ta=80.

Figure 15 illustrates the evolution of the dispersion coefficient (D) as a function of the power-law index (n) for Re=3 and Ta=80. The dispersion coefficient approach quantifies the non-ideal mixing and indicates the radial flow in the duct. A larger dispersion coefficient points to better mixing and lower dispersion coefficient suggesting a plug flow within the system. From the Fig. 15, we note that the dispersion coefficient decreases and exhibits a decreasing trend in the range of n between [0.6 and 0.9] with a minimal value about n=0.9. In addition, the dispersion coefficient is higher for a high axial Reynolds number. To further increase of the power-law index (n), we observe that the dispersion coefficient increases because of the higher apparent viscosity of the power-law fluid. As a result, when n increases, concentration gradients decrease along the radial direction consequently, the axial dispersion coefficient increases in the channel. Thus, high values of the dispersive coefficient correspond to a good mixing of dilatant fluids and non-ideal mixing of pseudoplastic fluids in the annulus. Similar results have been found in the form of tanks in series (N) in the Fig. 14.

Figure 16 illustrates the dispersion coefficient as a function of the radius ratio for different theological index behavior (n) for Ta=100 and Re=3. For a pseudoplastic fluid of n=0.6 the Fig. (16a) shows that the dispersive coefficient exhibits its lowest value for η=0.6. Above this value of the radius ratio, the axial dispersion coefficient increases indicating, thus, the good mixing increases for this kind of fluids. For the Newtonian fluid of n=1 in the Fig. (16b), the dispersion coefficient remains almost constant when the radius ratio increases above η=0.6. This behavior reveals that the mixing is not affected by the variation of the radius ratio. For the dilatant fluid of n=1.2 as illustrated in Fig. (16c), the dispersive coefficient decreases monotonically when the radius ratio (η) increases, reducing thus the mixing. Finally, for n=1.4 we note that the dispersion coefficient is higher for lower radius ratio and decrease when (η) increases.

5. CONCLUSION

In this study, we performed a numerical analysis based on the Lattice Boltzmann method to determine the effect of the power-law fluids flow structures on levels of mixing between two concentric cylinders where the inner cylinder is rotating while the outer cylinder is maintained at rest with an imposed laminar axial flow. A pulse

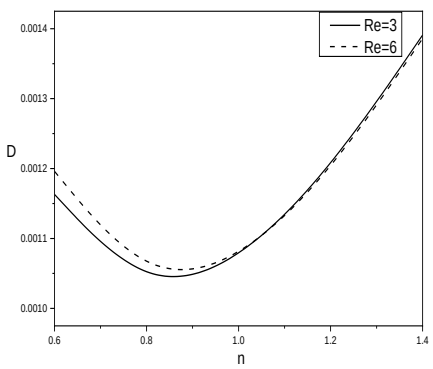

Fig. 15. Evolution of the dispersive coefficient for different fluids for Re=3 and Ta=80

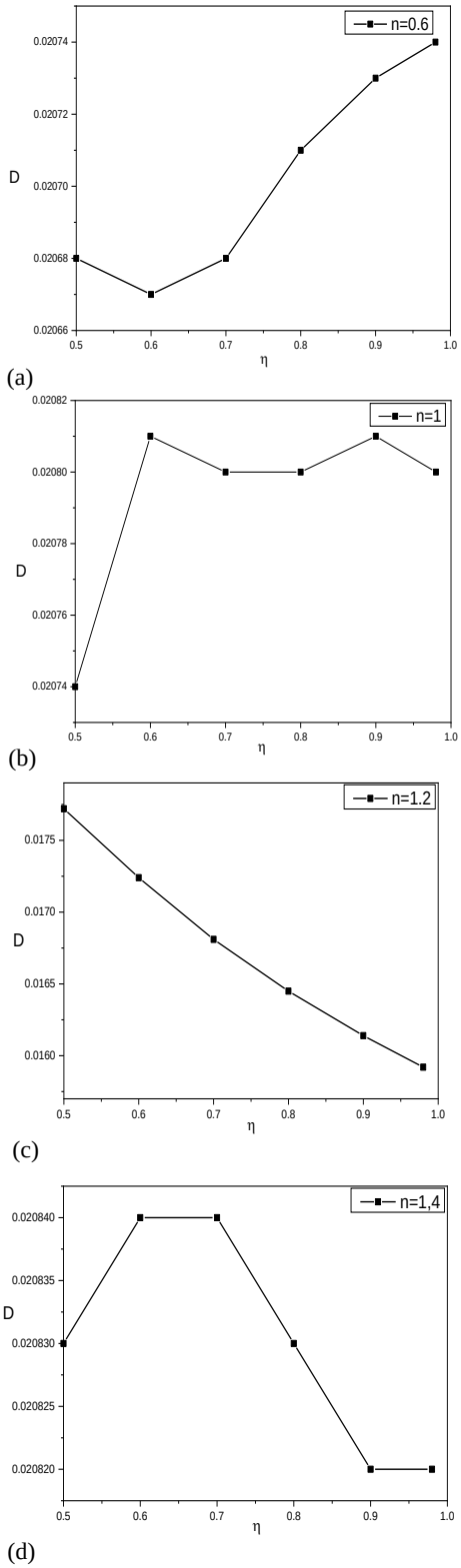

Fig. 16. Evolutions of the dispersive coefficient for different radius ratio and rheological index behavior (n) for Ta=100 and Re=3.

input injection of a tracer was computed at the outlet of the annulus. The residence time distribution and the mean residence time were used to determine the number of tanks in series and the axial dispersion coefficient to evaluate levels of mixing. As a main objective of this study, is to analyze the effect of the flow structure of a power-law fluid between two concentric cylinders on the mixing level and mean residence time in a Taylor-Couette system. The novelty of our work is the use of power-law fluids as particles-carrying fluids. The obtained results showed that the peak of the residence time distribution increases when the axial viscous forces increase and prevail on the centrifugal forces in the annulus, leading to a low level of mixing in the annulus. The axial flow with Re=3 dominates the secondary flow generated by the inner cylinder rotation for Ta=30 and, as a result, the mean residence time is slightly higher for fluids belonging to pseudoplastic family. For Re=6, the opposite trend is observed for pseudo-plastics fluids. For Re=3 and Ta=80 the area under curves of the residence time distribution increase when the power law index (n) increases leading to higher levels of mixing in the annulus. For Ta=100 and for both values of Re=3 and 6, when the power-law index increases, the number of stirred tanks in series (N) increases for pseudoplastic fluids family (n<1) indicating a lower levels of mixing and it decreases for dilatant fluids family (n>1) indicating a higher level mixing. For Ta=80 and Re=3, the increase of the power law index for pseudoplastic fluids leads to the decrease of the dispersion coefficient indicating the non-ideal mixing and for further increase of the power law index for dilatant fluids leads to the increase of the dispersion coefficient indicating the well mixing for dilatant fluids.

REFERENCES

Aparicio-Mauricioa, G., F. A. Rodrígueza, J. H. Joep Pijpersb, M. R. Cruz-Díaza and E. P. Rivero (2020). CFD modeling of residence time distribution and experimental validation in a redox flow battery using free and porous flow. *Journal of Energy Storage* 29, 101337

Baleo, J. N. and P. Cloirec (2000). Numerical simulation of the spatial distribution of mean residence time in complex flows through porous media. *Progress of Theoretical Physics Supplement* 138(690-695).

Bartak, M. I. Beausoleil-Morrison, J. A. Clarke, J. Denev, F. Drkal, M. Lain, I. A. Macdonald, A. Melikov, Z. Popiolek and P. Stankov (2002). Integrating CFD and building simulation. *Build Environ* 37 (8-9), 865-871.

Campero, R. and R. Vigil (1997). Axial dispersion during low Reynolds number Taylor-Couette flow: intra vortex mixing effect. *Chemical Engineering Journal* 52(19) 3305-3310.

Chanteloup, V. and P. S. Mirade (2009). Computational fluid dynamics (CFD) modeling of local mean age of air distribution in forced-ventilation food plants. *Journal of Food Engineering* 90(1), 90-103.

Danckwerts, P. V. (1958). The effect of incomplete mixing on homogeneous reactions. *Chemical Engineering Science* 8(1–2), 93-102.

Desmet, G., H. Verelst and G. Baron (1996). Local and global dispersion effect in Couette-Taylor flow-i. description and modeling of the dispersion effects. *Chemical Engineering Journal* 51(8),1299-1309.

Devi, M. and U.Gupta (2022). Stability analysis of binary casson nanofluid convection with viscosity and conductivity variations using darcy–brinkman model. *ASME Journal of Heat and mass Transfer* 144(12), 121201.

Devi, M., J. Sharma and U. Gupta (2022). Effect of internal heat source on Darcy-Brinkman convection in a non-Newtonian Casson nanofluid layer. *Journal of Porous Media* 25(4), 17-35.

Enkoida, Y., K. Nakata and A. Suzuki (1989). Axial turbulent diffusion in fluid between rotating coaxial cylinders. *AIChE Journal* 35(7), 1211-1214.

Guihard, I., F. Coeuret, L. Legrand, T. Fahidy and Z. Gu (1989). Circumferential mixing in the taylor-couette reactor. *Chemical Engineering Progress Symposium Series* 112, 105-117.

Guo, X. Y. Fan and L. Luo (2018). Residence time distribution on flow characterization of multichannel systems: Modeling and experimentation. *Experimental Thermal and Fluid Science* 99, 407-419.

Gyürkes, M. L. Madarasz, P. Zahonyi, A. Kote, B. Nagy, H. Pataki, Z. Kristof, N. A. Domokos and A. Farkas (2022). Soft sensor for content prediction in an integrated continuous pharmaceutical formulation line based on the residence time distribution of unit operations. *International Journal of Pharmaceutics* 624. 121950.

Haicheng, L., J. Wang, Z. Shu, G. Qian, X. Duan, Z. Yang, X. Zhou and J. Zhang (2022). Residence time distribution and heat/mass transfer performance of a millimeter scale butterfly-shaped reactor. *Chinese Chemical Latters* S1001-8417(22)00718-5.

Hwang, J. Y. and K. S. Yang (2004). Numerical study of Taylor–Couette flow with an axial flow. *Computers & Fluids* 33, 97-118.

Kataoka, K., H. Doi, T. Hongo and M. Futagawa (1975). Ideal plug-flow properties of Taylor vortex flow. *Journal of Chemical Engineering of Japan* 8(6), 472-476.

Kataoka, K. and T. Takigawa (1981). Intermixing over cell boundary between Taylor vortices. *AIChE Journal* 27(3), 504-508.

Kataoka, K., H. Doi and T. Komai (1977). Heat and mass transfer in Taylor vortex flow with constant axial flow-rate. *International Journal of Heat Mass Transfer* 20(1) 472-476.

Kaur, J., U. Gupta and R. P. Sharma. (2022). Nonlinear stability analysis for the rheology of Oldroyd-B nanofluids embedded by Darcy–Brinkman porous media using a two-phase model. *Proceedings of the Institution of Mechanical Engineers, Part E: Journal of Process Mechanical Engineering*.

Kaur, J. and U. Gupta (2022, July). Nonlinear analysis for thermal convection in Oldroyd-B nanofluids with zero nanoparticle flux on the boundaries. *Indian Journal of Physics* Online First.

Khali, S., R. Nebbali and K. Bouhadef (2017). Effect of a porous layer on Newtonian and power-law fluids flows between rotating cylinders using lattice Boltzmann method. Journal of the Brazilian Society of Mechanical Sciences and Engineering

Legentilhomme, P., L. Brujes and J. Legrand (1997). Distribution of staying times of liquid in a non-maintained liquid-solid edding flow: influence of the presence of solids. *Chemical Engineering Journal* 67(2) 83-96.

Legrand, J., F. Coeuret and M. Billon (1983). Structure dynamique et transfert de matière liquide –paroi dans le cas de l'écoulement laminaire tourbillonnaire de Couette-Poiseuille. *International Journal of Heat Mass Transfer* 26(7), 1075-1085.

Legrand, J. and F. Coeuret (1986). Circumferentional mixing in onephase and two-phase Taylor vortex flow. *Chemical Engineering Science* 41(1) 47-53.

Liu, M. Y. (2011). Quantitative characterization of mixing in stirred tank reactors with mean age distribution. *The Canadian Journal of Chemical Engineering* 89(5), 1018-1028.

Liu, M. and J. N. Tilton (2010). Spatial distributions of mean age and higher moments in steady continuous flows. *AIChE Journal* 56(10), 2561-2572.

Madeira, L. M., A. Mendes and F. Magalhaes (2006). Taching laminar-flow reactors: from experimentation to CFD simulation. International Journal of Engineering Education 22(1), 188-196.

Molki, M., K. N. Astill and E. Leal (1990). Convective heat-mass transfer in the entrance region of a concentric annulus having a rotating inner cylinder. *International Journal of Heat and Fluid Flow* (11), 2.

Moore, C. and C. Cooney (1995). Axial dispersion in Taylor-Couette flow. *AIChE Journal* 41(3), 723-727.

Nemri, M., S. Charton and E. Climent (2016). Mixing and axial dispersion in Taylor–Couette flows: The effect of the flow regime. *Chemical Engineering Science* 139,109-124.

Ohmura, N., K. Kataoka, Y. Shibata and T. Makino (1997). Effective mass diffusion over cell boundaries in Taylor-Couette flow system. *Chemical Engineering Journal* 52(11), 52-1757.

Pudjioni, P. and N. Tavare (1993). Residence time distribution analysis from a continuous Couette flow device around critical *Taylor Number*. *Chemical Engineering Journal* 48(2), 101-110.

Russ, D. C. and R. E. Berson (2016). Mean age theory in multiphase systems. *Chemical Engineering Science* 141(17), 1-7.

Shukla, S. and U. Gupta (2022). LTNE Effects on Triple-Diffusive Convection in Nanofluids, *ASME Journal of Heat and Mass Transfer* 144(9), 092501).

Tam, W. and H. Swinney (1987). Mass transport in turbulent taylor couette flow. *Physical Review A* 164(3), 1374-1381.

Theaker, N. (2017). *A Comparison of Mean Age Theory and Residence Time Distributions in Mixed Systems.* Electronic Theses and Dissertations, University of Louisville.

Wang, R., Z. Wang, X. Bi, C. J. Lim and S. Sokhansanj (2022). Residence time distribution and solids mixing of sawdust in a horizontal pulsed fluidized bed. *Powder Technology* 397, 117006.

Zhang, G. T., N. Wannenmacher, A. Haider and O. Levenspiel (1990). How to narrow the residence time distribution of fluids in laminar-flow in pipes. *The Chemical Engineering Journal* 45(1), 43-48.

Zhou, J. G. (2011). Axisymmetric lattice Boltzmann method revised. *Physical Review E* 84, 036704.

Zhu, X., R. Campero and D. Vigil (2000). Axial mass transport in liquid Taylor-Couette-Poiseuille flow. *Chemical Engineering Science* 55(21), 5079-5087.